
Article:
Mullis, A (2019) The Physical Mechanism for Melt Pulsation During Close-Coupled Atomization. Atomization and Sprays, 29 (2). pp. 143-159. ISSN: 1044-5110

https://doi.org/10.1615/AtomizSpr.2019030110

The Physical Mechanism for Melt Pulsation During Close-Coupled Atomization

Andrew M. Mullis

School of Chemical & Process Engineering, University of Leeds, Leeds LS2 9JT, UK

Abstract

High speed filming (18000 fps) has been used to study the phenomenon of melt pulsation in a discrete jet, high pressure gas atomization system. Image processing routines have been developed to determine the velocity of material within the melt plume as it streams away from the melt delivery nozzle and to parameterise the shape of the melt plume. This data is then correlated with the volume of material in the melt plume, which is used as a diagnostic for melt pulsation. We find that during periods of low melt the constriction in the melt plume in which its diameter is a minimum is smaller and further downstream. Both appear to be consistent with a transition from an open-wake structure during periods of high melt flow to a closed-wake during periods of low melt flow. Moreover, the average velocity of material in the plume appears to drop during periods of low melt flow, which we ascribe to its passage through the Mach disk. We conclude that there is sufficient evidence to assert that the closed-wake condition survives the introduction of a dense second fluid to the atomizer and that alternation between the open- and closed-wake condition is the likely cause of the observed melt pulsation.

Keywords: Gas Atomization, Melt Pulsation, High Speed Video, Object Tracking

1. Introduction

Close-coupled gas atomization is used extensively for the production of powder metals, in particular where fine ($d_{50} \leq 50$ μm) or highly spherical particulates are required such as in Additive Layer Manufacturing (ALM) processes. However, the particles size distribution (PSD) of powders produced by gas atomization tends to be quite broad, typically spanning an order of magnitude or more (Anderson and Terpstra, 2002). This in turn leads to high scrappage/remelt rates for applications that require a narrow size distribution. For powder producers supplying demanding markets, such as for ALM feedstock, the remelt rate may be as high as 65%, wherein significant cost saving could result from even modest improvements in control of the particle size distribution. There exists a significant body of literature detailing various instabilities that occur during close-coupled gas atomization and how these may impact on the application of such powders as ALM feedstock (see e.g. the recent review by (Anderson et al., 2018)). The corollary of this is the prospect that if the stability of the atomization process could be improved, then a superior powder produce could be offered.

One of the most common such instabilities is that of melt pulsation, in which the amount of melt instantaneously being delivered to the melt nozzle varies chaotically. When high melting point metals are atomized this can be observed with the naked eye as a flickering of the intensity of the atomization spray cone. Mullis et al. (2013) estimated that such pulsation can cause the gas-to-metal ratio (GMR = $\dot{m}_g / \dot{m}_m$, where $\dot{m}_g$ is the mass flow rate of gas and $\dot{m}_m$ is the mass flow rate of metal) to vary between 1.26 (kg gas/ kg melt) and 15.16 over periods < 1 s. Given the well-established correlations between median particle size and the GMR (e.g. Lubanska, 1970), it is difficult to envisage that large, short-duration fluctuations in the melt flow rate could not but effect the particle size distribution.

The pulsation phenomenon was first formally described by Ting et al. (2002), with Fourier analysis of high speed filming subsequently being used (Ting et al., 2005; Mullis et al., 2008) to confirm that the dominant frequencies present are typically < 25 Hz. Based upon their observations Ting et al. (2002) proposed the so-called pulsatile model, suggesting that pulsation results from a chaotic oscillation between the open- and closed-wake conditions. The wake region occurs due to the separation of the supersonic flow from the melt nozzle's edge, and is characterised by a recirculating subsonic gas flow. It is delineated from the rest of the flow by an internal sonic boundary. The far end of the wake region is determined by the position of the 'stagnation point', a point of maximum pressure and minimum velocity where the majority of the gas enters the wake region. The structures of the open- and closed-wake are shown schematically in **Figure 1**. These have been traced to scale from Schlieren images of open- and closed-wake flow as obtained by Mates and Settles (1995). As such they accurately represent the structure and scale of the primary features observed in the open- and closed-wake. The very obvious recirculation zone immediately below the nozzle in the open-wake case appears absent in the closed-wake case. CFD modelling (Motaman et al. 2015) suggests that in fact a recirculation zone is still present, but is much reduced in size.

In gas-only flow the open-wake condition is stable at low pressure. Upon increasing the gas inlet pressure the structure of the flow-field goes through some changes. The internal shocks caused by the expansion of the issuing gas moves downstream. With increasing inlet pressure they continue to move further downstream such that the recompression shock reflected from the internal sonic boundary crosses the rest of the recompression shocks to form a Mach disk (Anderson et al., 1991). The formation of the Mach disk cuts off the wake region from the surrounding gas flow, dramatically decreasing its size and strength. This phenomenon is termed 'wake closure', with the closed-wake condition also being stable in gas-only flow.

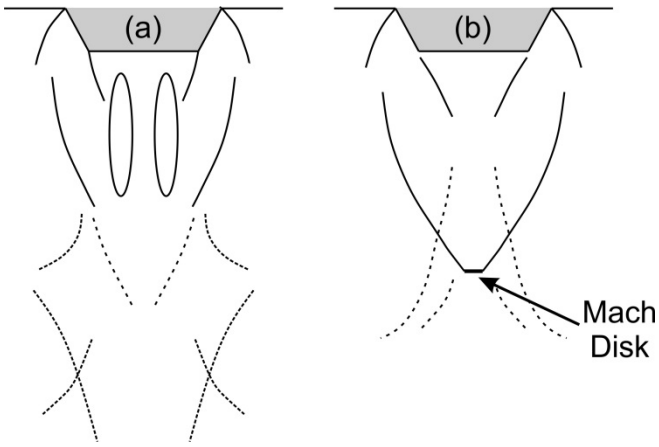

Figure 1. Gas flow structures in (a) the open-wake and (b) the closed-wake condition during gas atomisation. Drawings produced to scale by tracing Schlieren images as given by Mates & Settles (1995). Lines represent the boundaries between light and dark regions in the Schlieren images, with the line type (solid, close-dashed, dashed) being indicative of the contrast gradient in the image.

The proposition made by Ting et al. (2002) is that a dynamic balance exists between the momentum of the melt and the momentum of the atomizing gas. In the closed-wake condition the high back pressure created by the separation of the wake region from the surrounding flow causes the melt flow rate to slow. However, the introduction of melt into the recirculation zone acts against the compressible gas, distorting and displacing the established flow features. As melt accumulates in the recirculation zone the Mach disk is disrupted. The system flips into the open-wake configuration causing a sudden drop in back pressure, with a commensurate increase in melt flow rate. With the release of melt from the recirculation zone the Mach disk is re-established and the cycle starts again. Consequently, the closed-wake may be categorised as a state of low melt flow rate, while the open-wake is a state of high melt flow rate, with pulsation being a chaotic oscillation between these two quasi-stable states.

However, the model is far from universally accepted. In particular Mates and Settles (2005a, 2005b) have argued, based on extensive Schlieren imaging studies of atomizers in single and two-phase flow, that wake-closure is not possible during two-phase flow. Specifically, they

state that wake closure is of no real consequence in atomization as the closed wake structure is not preserved during the actual atomization process. The introduction of the dense melt disturbs the shock wave structure, causing the disappearance of the Mach disk, and the 'opening' of the wake. Consequently, the basis for the pulsatile model of Ting et al. (2005), they argue, is incorrect.

The origin of the pulsation phenomenon has been one of the area of atomization research that modelling using Computational Fluid Dynamics (CFD) has been unable to shed light on. A number of CFD models have been constructed for various atomizer geometries, but the complexity of the 2-fluid problem has meant that such studies have typically been restricted to gas only flow. Such studies have reproduced the essential features of the open- and closed-wake structure (Ting and Anderson, 2004), permitted the aspiration effect and position of the Mach disk to be characterised as a function of gas pressure (Xinming et al., 2009) and demonstrated that even relatively small changes to the configuration of the melt nozzle and gas manifold can lead to significant changes in the pressure required for wake closure (Motaman et al., 2015).

In this paper we present a suite of new methods for analysing high speed video footage obtained during close-coupled gas atomization. The tools are designed to parameterise the shape of the atomization plume and to determine the velocity of material within the plume. By correlating these melt plume statistics against the pulsation behaviour of the atomizer we are able to draw conclusions regarding the physical mechanism responsible for pulsation.

2. Experimental Methods

2.1 Atomization Experiments and Filming Procedure

Gas atomization experiments were performed using a close-coupled gas atomizer as supplied by a commercial manufacturer of both research and production scale gas atomizers. The system, which can atomize 10 kg batches of material at a time, is of the discrete jet design in which 18 jets of 0.5 mm diameter were arranged concentrically around a central melt delivery nozzle. The apex angle at the focus of the jets was 45°. Melt was fed down the central, 2.5 mm diameter, bore of the nozzle before wetting the flat nozzle tip, the diameter of which was 5.0 mm. The arrangement, which is similar to both the USGA (Anand et al., 1978) and Ames HPGA-I (Anderson et al., 1991) designs, is shown schematically in **Figure 2**.

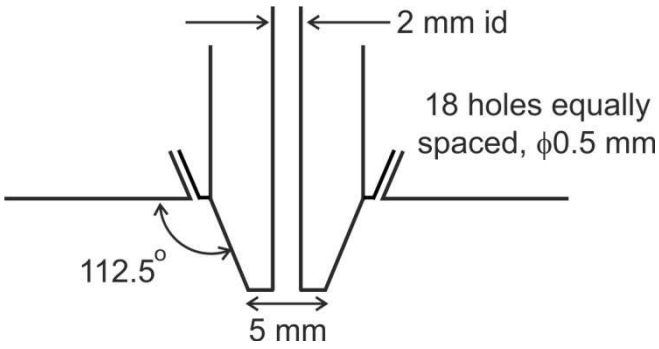

Figure 2. Schematic diagram of the gas atomisation nozzle used in the high speed filming experiments.

In the experiment reported here the atomized fluid was an Al-31.5 at.% Ni melt, the liquidus temperature of which is 1613 K. Atomization was performed at 1813 K, giving a 200 K melt superheat, wherein the atomized melt plume was sufficiently bright for all filming to be performed in the radiant light emitted by the melt. The atomizing gas was Ar, with the manifold pressure being 3.5 MPa, giving an estimated gas flow rate of 0.0487 kg s^{-1}. In order to ensure a steady flow of melt to the atomizer the tundish sitting above the melt delivery nozzle was pressurised to 40 kPa with Ar gas. This is necessary as the aspiration pressure, the pressure just below the melt nozzle in gas only flow, for a gas pressure of 3.5 MPa is slightly (12 kPa) above

ambient. That is, the system does not naturally aspirate so as to draw melt into the atomizer, the melt flow is forced via pressurisation of the tundish. This may make this configuration susceptible to small variations in the pressure at the melt nozzle. The time averaged melt flow rate during the experiment was 0.0158 kg s^{-1}, giving an average gas-to-metal ratio (GMR) of 3.08 (kg gas to kg melt). The ultimate d_{50} particle size in the collected powder was 59.7 μm.

High speed filming was performed using a Kodak Ektapro 4540mx High Speed Digital Motion Analyser operating at a frame rate of 18,000 fps. The camera was fitted with a Micro-Nikkor 70-180 mm zoom lens allowing a 42 mm field of view at the atomizer nozzle from a working distance of around 0.3 m. However, in practise the useful viewing distance was typically limited to 30 mm downstream of the nozzle, as cooling of the melt plume meant that beyond this distance the plume was too faint to be resolved. This gives a spatial resolution of 0.17 mm per pixel. Total filming time was limited to 3.64 s due to a storage limitations, with a maximum of 65536 frames being buffered on the camera before filming had to be stopped and the data downloaded to a control PC.

2.2 Previous Analysis Methods

A schematic diagram illustrating the main features of the melt plume geometry is shown in **Figure 3**. Upon exiting the melt nozzle the melt plume first contracts, forming a 'throat', a region of minimum diameter, located close to the focus of the converging gas jets. The location of this throat region is designated as being a distance z_t downstream of the outlet nozzle, with a diameter d_t. Beyond the throat region the melt plume increases in size eventually reaching a near constant diameter which is maintained until the plume fades below the detection threshold of the camera.

This atomizer configuration has previously been studied extensively by Mullis et al, (2008, 2013). In Mullis et al. (2008) a narrow window of width *w* pixels, located *m* pixels below the tip of the melt delivery nozzle was defined. This is also shown in **Figure 3**. In Mullis et al. (2008) the width of the window, *w*, was taken as four pixels, and the window was located at *m* = 5 pixels below the melt outlet nozzle. For consistency, these values are also adopted here. The basis of the analysis presented in Mullis et al. (2008) was to average the optical intensity over the pixels sampled in the window and use this average optical intensity, I_m^n, as a proxy for the amount of melt instantaneously flowing from the nozzle. Here where *n* labels the frame from which the data was extracted and *m* labels the position on the *z*-axis where the sampling window was located. The association of melt-flow with optical intensity will be approximately valid provided that: (i) the melt undergoes minimum cooling prior to being sampled, (ii) the melt undergoes relatively uniform breakup prior to being sampled, (iii) there is no saturation of the pixels being sampled. Assumptions (i) & (ii) are met by having the sampling window very close to the melt outlet nozzle, the validity of assumption (iii) will be confirmed below. Moreover, we claim only a general correlation between the volume of melt being instantaneously delivered to the melt nozzle and the measured optical intensity, i.e. that low brightness equates to low flow rate and high brightness to high flow rate. In particular, it is unlikely that there is a linear relationship between optical intensity and melt flow-rate. However, we are unable to measure the time resolved melt flow-rate to establish this relationship more definitively.

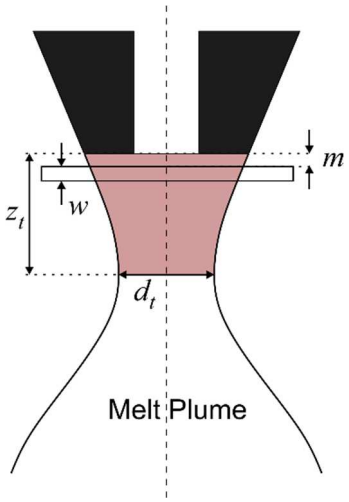

Figure 3. Schematic diagram of the melt plume geometry showing the throat region of diameter d_t, located a distance z_t below the melt nozzle. For the analysis described in Section 2.5 the melt in the wake region is the region shown shaded between the melt nozzle and the throat. Also shown, sampling window w pixels wide located m pixels below the nozzle outlet.

The analysis of Mullis et al. (2008) unambiguously demonstrated two important characteristics of the melt flow during gas atomization. The first was a relatively high frequency (300 Hz) instability which appeared to be due to precession of the melt. This was apparent as a regular left-right swinging motion of the melt plume in the 2D imaging plane. **Figure 4** illustrates this by showing two frames from the high speed movie, with the melt plume (a) displaced to the left as viewed and (b) displaced to the right as viewed. The total time between the images shown in **Figure 4a** and **Figure 4b** was 1/600 s, this being consistent with the 300 Hz frequency for a full left-right-left cycle to be completed. This type of instability had previously been observed by Anderson et al. (2006) who ascribed it to incomplete wetting of the nozzle tip by the melt, an observation subsequently confirmed by direct observation of the melt filament using ultra-high speed imaging with a 20 ns pulsed laser (Mullis et al., 2011).

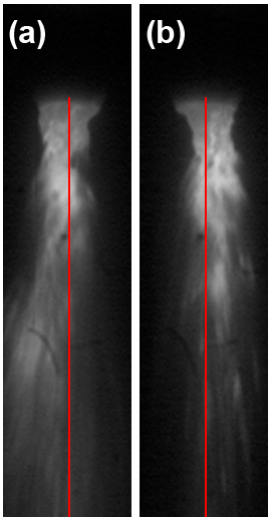

Figure 4. Frames (a) 5279 and (b) 5309 from the high-speed filming of the atomisation process showing precessional motion of the melt plume as a left-right swinging of the plume. Time between the frames is 1/600 s. Red line indicates centre of the melt nozzle, which may not coincide with the centre of the image frame.

The second was a chaotic pulsation in the melt volume being instantaneously discharged from the nozzle. Typically, most of the spectral power was restricted to the frequency range 5-30 Hz, but unlike the precessional instability, there was no one single dominant frequency. **Figure 5** shows the optical intensity (0-255 scale) averaged over a window located at $m = 5$, i.e. 5 pixels (0.86 mm) below the melt delivery tip.

The superimposed precessional motion does have a minor effect on the measured brightness as the melt plume swings towards and away from the camera. It is shown in Mullis et al. (2008) that this takes the form of a low amplitude oscillation superimposed upon the main pulsation trend. However, due to the very regular nature of the precessional motion at 300 Hz this is easily filtered out. Here we have used a digital low pass filter to smooth the resulting time-series data and remove the high frequency signature of the precessional motion of the melt. This is an infinite impulse response filter of the Butterworth type with a pass-band of $f < 40$ Hz

and a -80 dB cutoff of $f > 200$ Hz. Further details of the filter design and application are given in Mullis et al. (2013).

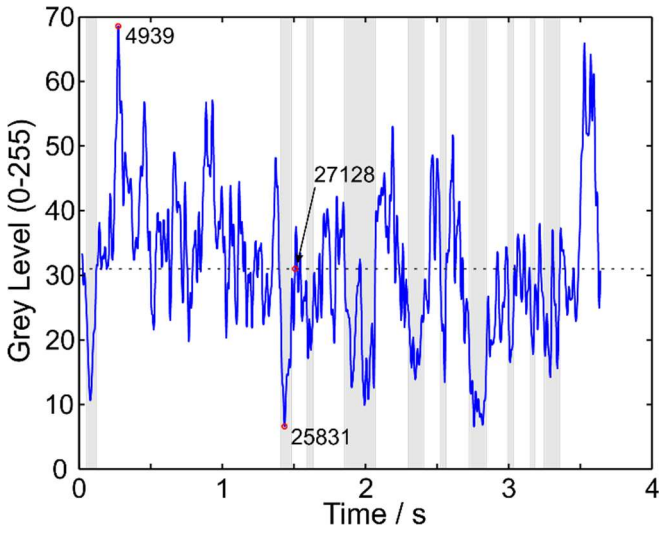

Figure 5. Mean grey level determined within a sampling window 4 pixels wide, situated 5 pixels below the nozzle outlet. Data is determined from each of the 65536 frames in turn and presented here as a time series. Vertical grey bands delineate regions of low recorded grey level corresponding to low melt flow. Dotted line indicates the mean grey level, circles indicate the maximum and minimum intensities (with their associated frame number) and one frame representative of the mean grey level.

The results show a very significant variation in the amount of material instantaneously at the melt nozzle. The mean brightness over the 3.64 s of recording was 31.03 (on a 0-255 intensity scale) with a standard deviation of 11.14. A feature of particular interest, as noted by Mullis et al. (2013), are the periods during which flow becomes very low, in some cases almost shutting off completely. The most obvious low flow periods are indicated on the Figure by the regions shaded light grey. The mean intensity within these regions is 16.95, around half the average global average. By way of comparison, the mean brightness measured outside of these regions is 35.28.

To illustrate what this means during filming **Figure 6** shows three frames from the high-speed video. **Figure 6a** is frame 4939, which has the highest mean intensity in **Figure 5**. As an aside, we note that even in this frame the maximum grey-scale value of any pixel within the image is 206 (0-255 scale). Hence, we assert with confidence that pixel saturation is not an issue in this analysis. Conversely, in **Figure 6b** we show frame 25830, which is identified as having the lowest mean intensity in **Figure 5**. Finally, by way of comparison, **Figure 6c** shows frame 27128, which has a mean intensity of 31.01, close to the global mean value obtained from **Figure 5**. From **Figure 6**, the extent to which the flow of melt is almost shut off during periods of low flow is clear and we consider it unlikely that variations of such magnitude could have a cause other than commensurate variation in the melt flow-rate.

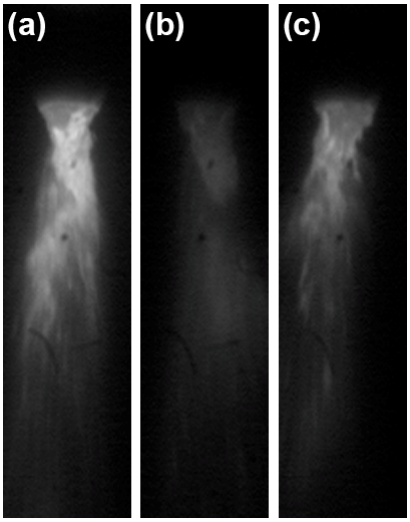

Figure 6. Three frames from the high-speed movie, (a) frame 4939, the brightest in the set, (b) frame 25831, the darkest in the set and (c) frame 27128 which is representative of the time-averaged mean grey level. Exposure settings are identical for all three images. The superimposed precessional motion is evident with (a) being almost central, (b) being displaced to the right as viewed and (c) being displaced to the left.

This level of pulsation is quite extreme and may be a consequence of the discrete jet type arrangement used on this atomizer. Specifically, because the discrete jet design reduces gas

consumption it is feasible to run such atomizers at higher pressure than conventional annular slit type designs, wherein the higher operating pressure may induce more severe pulsation. Nonetheless, given the interest in discrete jet type designs for the economical production of ultrafine powders (Anderson & Terpstra, 2002) and this being a commercial atomize, we consider this to be an interesting design to investigate.

However, our contention here is that such high speed video contains a much richer data set and that this can be used not only to demonstrate atomizer pulsation, but to elucidate the physical processes giving rise to that pulsation. Here we focus on two characteristics of the plume, the velocity of material contained within it and the geometry of its outer envelope.

2.3 Melt Plume Velocity

Based on identifying a particularly distinctive feature within the melt plume and tracing its progress across several consecutive frames, Mullis et al. (2008) were able to estimate the velocity of the melt within the plume. They gave this as approximately 30 m s^{-1}. However, this was based upon a single spatial location and a given instant in time. In principle, such a process could be formalised and automated so as to determine the velocity of material within the plume with both spatial and temporal resolution.

An extensive literature has built up in the field of computer vision which relates to such problems, namely: how do we track objects as they move across consecutive frames within a movie sequence. The approaches adopted within the computer vision literature may be classed as adopting either a Fourier (e.g. Ejiri and Hamada, 2006) or non-Fourier (e.g. Malavika and Poornima, 2013) approach. However, in both cases we describe the computer vision approach as being deterministic in that the algorithm attempts to accurately track features, be they cars,

human faces or manufactured parts on a production line, which change their appearance relatively little between consecutive frames. In fact, this is likely to be a poor assumption for features within an atomization plume for a number of reasons:

1) As a consequence of the spatial expansion of the plume, features observed close to the melt nozzle will become more diffuse as they progress downstream;
2) The brightness of features within the plume will decrease continuously with distance downstream, due to cooling of the melt in the much colder gas stream;
3) It is likely that there will be differential velocities present within the plume, meaning that features that were co-located near the nozzle outlet may not remain so as they travel downstream;
4) We are projecting a 3-dimensional spray plume onto a 2-dimensional imaging plane, wherein features may be obscured as they cross in front of, or behind, each other;
5) Features within the plume, which are typically aggregates of co-moving particles, may merge with other features or fragment.

Consequently, traditional computer vision algorithms struggle to reliably determine and track features within an atomization spray plume.

For the reasons outlined above we have adopted here a more statistically based approach, based on the cross-correlation of an image pair. Similar techniques are described by Tokumaru & Dimotakis (1995) and by Duke et al. (2010), who used the technique to study the breakup of an annular liquid sheet. To illustrate the principle consider the idealised case in which a set of well defined, discrete features are formed at the nozzle tip and then move downstream at constant velocity and in a shape preserving manner. At some instant in time corresponding to frame n we will have a pixel profile I_m^n which will correspond to the set of feature as they pass pixel row m. Sometime later, at frame $n + i$, these features will have moved downstream by j

pixels such that pixel vector I_{m+j}^{n+i} will be identical to I_m^n. In this case the correlation coefficient between I_m^n and I_{m+j}^{n+i} will be 1. Of course, the situation we have described is far from the reality of an atomization plume. Notwithstanding this, we conjecture that if we take *i* sufficiently small, we can identify the *j* such that I_{m+j}^{n+1} corresponds to the same set of features as represent by I_m^n at the earlier time. To do this we calculate the cross-correlation between I_m^n and all I_{m+j}^{n+1} for $1 \le j \le J$, searching for the maximum correlation between the two vectors. At the *j* corresponding to the maximum correlation we assume that we have tracked the features between consecutive frames and can assign an average displacement between frames. Knowing the time-base between frames this may be converted to an average velocity for all features in that horizontal pixel row. Moreover, the value of the maximal correlation coefficient can be used to determine the level of confidence with which the assignment of the displacement is made. Here *J* is the maximum number of pixels downstream which is searched for a match. The appropriate value of *J* is determined by trial and error, although the results are insensitive to the value chosen provided *J* is sufficiently large. Here we have terminated the search when $J = 30$ or when the plume becomes too faint for the features to be resolved.

Using the procedure outlined above the time resolved velocity of the plume at a given horizontal level can be determined by scanning though *n* whilst keeping *m* fixed. Conversely, a spatially resolved velocity profile moving downstream through the plume can be obtained by fixing *n* and scanning through *m*. Generally, a good match can be found between I_m^n and an appropriate I_{m+j}^{n+1}. In the case $m = 15$ (i.e. the initial sampling window is 15 pixels or 2.6 mm below the nozzle outlet), the value of the maximum correlation coefficient (i.e. at the point where I_m^n and I_{m+j}^{n+1} are deemed to match so that a velocity can be determined) averaged over all 65536 frames was 0.9456, with a standard deviation of 0.0160. Further downstream the

mean (standard deviation) are 0.9733 (0.0071) at m = 35 (6.0 mm below the nozzle outlet) and 0.9772 (0.0053) at m = 55 (9.5 mm below the nozzle outlet). For comparison the statistically significant value, based on a one-tailed t-test with a number of degrees of freedom equal to the size of the I vector – 2, is 0.2902 at the 1% significance level. From this we conclude that provided i is small, and here we only consider the case of i = 1 (i.e. δt = 1/18000 s) the algorithm for velocity determination appears robust.

2.4 Plume Envelope Geometry

The velocity of the material being transported in the plume is not, however, the only information that may be extracted from the high speed video sequence. The geometry of the plume envelope may also be determined and parameterized, with the information thus obtained being used to help elucidate the physical processes giving rise to atomizer pulsation. The process is relatively straightforward. First a threshold intensity level, I_{thr}, is set. I_{thr} may be either an absolute grey level (e.g. intensity = 45 on the 0-255 scale output of the camera) which is applied to all frames, or it may be a relative level obtained on a frame by frame basis. In the latter case the maximum and minimum intensity levels, I_{max} and I_{min}, within each frame are determined and I_{thr} set for the frame in question according to

$$I_{thr} = I_{min} + \lambda(I_{max} - I_{min}) \qquad (1)$$

where $0 \le \lambda \le 1$ is constant, and Equ. (1) allows for some frames having a non-zero background grey level. In general, because the volume of melt discharged by the atomizer varies in time, thus leading to significant variations in the maximum intensity between frames, the relative approach to setting I_{thr} as defined by Equ. (1) is preferred, with λ typically assigned a value of 0.2-0.3.

Starting at the z-position corresponding to the nozzle tip we then scan from both low-x and high-x to determine the first location in each case where the actual grey level exceeds I_{thr}. This determines the locus of the melt plume at this z position, wherein we move 1 pixel downwards in z and repeat the process, building up the entire locus of the melt plume. The downward scan of the frame is terminated at the point where no pixels exceed the I_{thr} grey level, with the procedure then being repeated for the next frame in the video sequence.

Figure 7 shows a typical frame (frame number 17575, t = 0.9764 s). In part (a) of the Figure we show the frame as captured, in part (b) the same frame with the locus of the melt plume, as identified by the routine, superimposed in red for $\lambda = 0.3$ and in green for $\lambda = 0.2$. In both cases it is evident that the routine identifies the location of the outer envelope of the plume in a reliable manner, with $\lambda = 0.3$ picking out the central region of the plume and $\lambda = 0.2$ tending to include more of the peripheral spray streaming off from the central plume. However, it is also evident that there are some darker areas inside the identified locus, although at the moment we seek to identify only the outer envelope of the plume and do not concern ourselves with characterizing the structure within the plume.

The plume geometry shows a constriction, referred to sometimes within the atomization literature as the throat, somewhat below the nozzle outlet. For the frame shown this is around 3.7 mm (0.73 nozzle diameters) below the tip, where the plume width is a minimum of 3.5 mm (0.70 nozzle diameters) for $\lambda = 0.3$ or 4.1 mm (0.82 nozzle diameters) for $\lambda = 0.2$. The plume width subsequently opens up as it progresses further downstream, eventually reaching a near steady value before detection is lost, which is indicated as a closing of the detected plume locus. In the analysis presented below we have extracted the width of the plume at the constriction point and the z-coordinate of the constriction, as two useful parameters which may be used to

understand the flow. The location of the throat is not found to sensitive to λ. The absolute value of the throat diameter detected does vary somewhat with λ and here we report values determined with $\lambda = 0.3$. However, the trends found (e.g. the way in which throat diameter correlates with measured optical intensity within the plume) are not sensitive to the choice of λ.

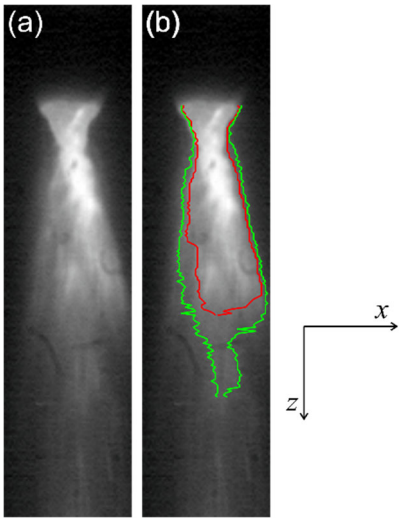

Figure 7. Typical frame from the high speed filming of the melt plume during gas atomisation showing (a) the location of the sampling window *m* pixels below the nozzle and its width, *w*, (b) the frame as captured and (c) with the outline of the plume as determined by the automated plume detection routine for $\lambda = 0.3$ (inner) and $\lambda = 0.2$ (outer).

2.5 Near Nozzle Melt Accumulation

Having identified the location of the throat region and the outer locus of the plume envelope one final calculation is performed. The pixels inside the envelope above the throat (the region shaded in **Figure 3**) are summed in order to calculate the cumulative optical intensity for material in the region between the nozzle and throat. As above, this is taken as a proxy for the amount of material in this region.

3. Results

3.1 Melt Plume Velocity

The time-resolved velocity of the material in the plume is shown in **Figure 8** for two values of *m*, *m* = 5 (0.86 mm below the nozzle tip, the location where the reference brightness is measured) shown in blue and *m* = 50 (8.6 mm below the nozzle tip) shown in red. For reference the grey regions shown on **Figure 5** indicating periods of low flow have been transposed onto **Figure 8**. That is, the highlighted regions shown in **Figure 8**, and in subsequent figures, are derived from the data shown in **Figure 5** and are indicative of periods of low melt flow, allowing for direct comparison with the melt flow rate. A number of features are worthy of note. Firstly, and perhaps most obviously, there is a very strong correlation between the volume of material at the melt nozzle and the flow velocity measured at this location (blue curve in **Figure 8**), with the correlation coefficient for the two data sets being 0.8584. In particular, the periods of low flow volume also correspond to periods of abnormally low flow velocity within the plume, as shown by the coincidence of low flow velocity with the shaded regions from **Figure 5**. The average flow velocity in the shaded regions is 17.0 m s^{-1}, compared with an average of 34.1 m s^{-1} outside of these regions.

The second striking feature of the results shown in **Figure 8** is the extent to which the estimated flow velocity has dropped by *m* = 50, 8.6 mm downstream of the nozzle tip. More specifically, for those times at which the flow velocity was high near the nozzle tip, the velocity has dropped significantly, typically from 30 – 40 m s^{-1} to 10 – 15 m s^{-1}. Conversely, for those times at which the velocity was already low near the nozzle tip, the velocity remains almost constant at 10 – 15 m s^{-1}, such that at *m* = 50 the temporal variation in velocity is almost eliminated.

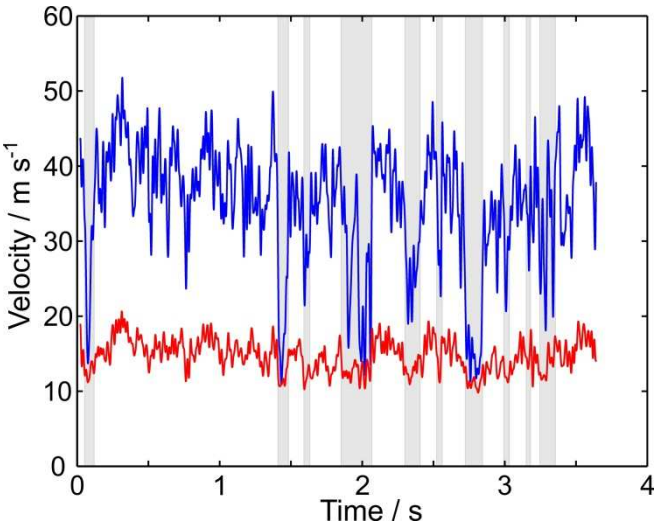

Figure 8. Vertical component of velocity of the melt plume measured at m = 5 (0.86 mm, upper curve) and m = 50 (8.6 mm, lower curve) below the melt nozzle. Vertical grey bars are adopted from Figure 5 and represent periods of low mean grey level (low melt flow rate).

This spatial variation in velocity is explored in more detail in **Figure 9**, in which we show the velocity as a function of distance downstream averaged over two short time periods, each of which corresponds to an interval of 400 frames (0.022 s). One of these, centered on frame number 15550 (t = 0.864 s) corresponds to an interval of high melt flow, the other centered on frame number 49550 (t = 2.753 s) corresponding to an interval of low melt flow. For comparison, the spatially resolved velocity averaged over all 65536 frames is also shown. In the high flow regime, the velocity drops essentially linearly with distance downstream for the first 9.5 mm or so, thereafter remaining approximately constant until the plume becomes too faint to resolve. In contrast, in the low flow regime, as is already apparent from **Figure 8**, the velocity is low throughout its downstream passage, with any initial decrease in velocity restricted to the first 2 mm or so downstream from the nozzle. As the atomizer spends the majority of its time in the high melt flow condition, the average over all frames is dominated by, and thus closely resembles, the high flow rate curve.

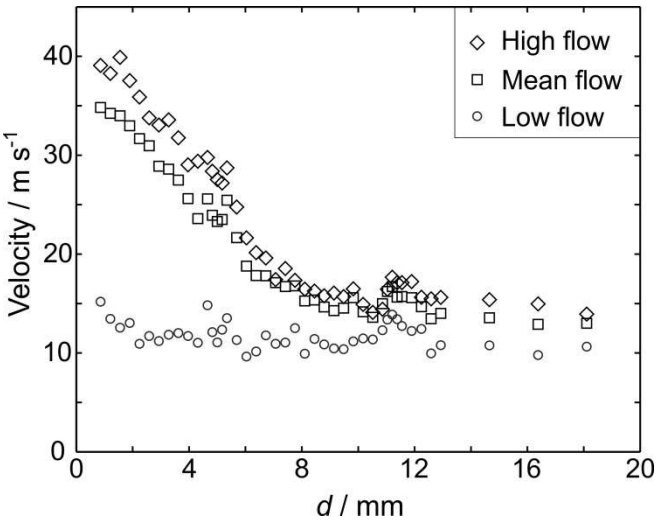

Figure 9. Time averaged velocity as a function of position with the atomiser in the high-flow (diamonds) and low flow (circles) conditions. In each case the average is determined over 400 consecutive frames. Also show (squares) is the global average over all 65536 frames.

3.2 Melt Plume Geometry

The minimum diameter of the constriction, or throat, in the melt plume, as a function of time is shown in **Figure 10** and its corresponding position in **Figure 11**. As previously, the shaded regions on the figures indicate periods of low melt flow, as determined from **Figure 5**. The data is obtained based on a relative threshold intensity determined on a frame-by-frame basis according to Equ. (1), with a value of $\lambda = 0.3$. As such, the average optical intensity (grey level) within the frame should not bias the throat determination. It is clear from **Figure 10** that throat diameter correlates well with the estimated melt flow rate as determined from the optical intensity near the melt delivery nozzle, with periods of low flow corresponding to times during which the throat is at its narrowest. Specifically, for the periods shown shaded in **Figure 10** the average throat diameter is 3.25 mm, compared with an average during the rest of the filming period of 3.79 mm. The linear correlation coefficient between the data for optical brightness and throat diameter is 0.4988.

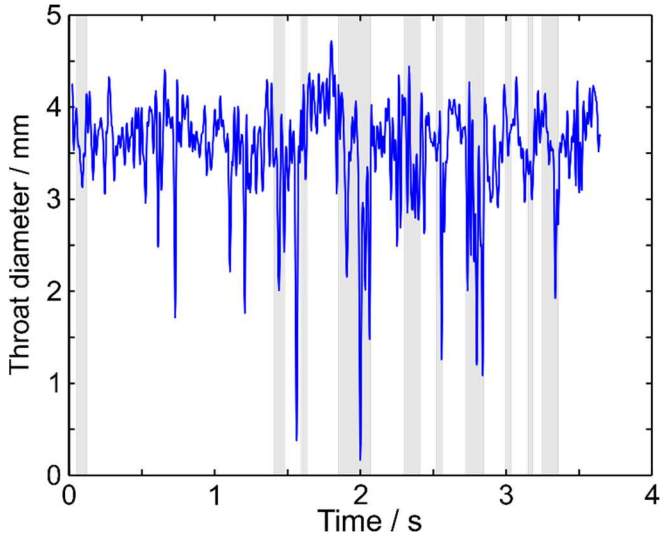

Figure 10. Diameter of the throat region of the melt plume. Vertical grey bars are adopted from Figure 5 and represent periods of low mean grey level (low melt flow rate).

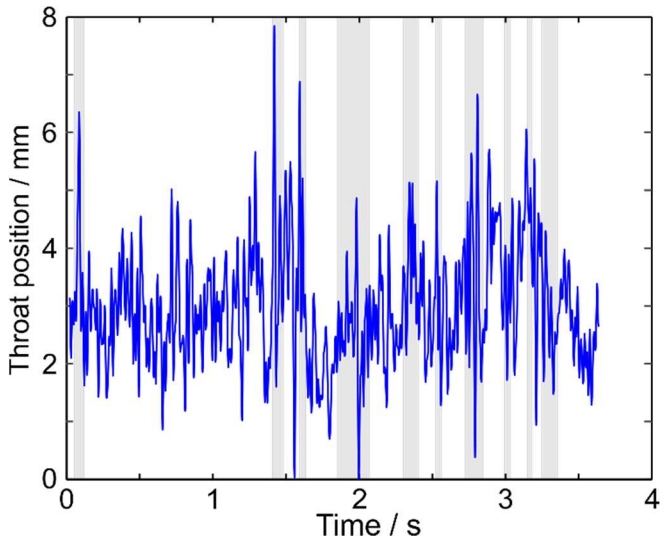

Figure 11. Location of the throat region of the melt plume, measured downwards from the melt nozzle outlet. Vertical grey bars are adopted from Figure 5 and represent periods of low mean grey level (low melt flow rate).

Conversely, with reference to **Figure 11**, it appears that the throat position, measured in distance downstream from the nozzle tip, is inversely correlated with the estimated melt flow rate, with the throat being further downstream during periods of low flow. The average downstream distance of the throat during periods of low flow is 3.80 mm, compared with 3.17 mm during the rest of the filming period. The linear correlation coefficient between the data

for optical brightness and throat position is -0.4059. For both the throat diameter and throat position we note that the correlation with the optical brightness data is somewhat weaker than is the case for the velocity data, although we also note that all are statistically significant. In fact, for such a large dataset (N > 65000) any correlation coefficient exceeding 0.009 would be considered significant at the 1% significance level (based on a one-tailed test).

3.3 Near Nozzle Melt Accumulation

Figure 12 shows the cumulative optical intensity for the material in the plume between the nozzle and the throat. The general tendency is for the cumulative intensity in this region to be low when the melt flow is low. In deed, there is a very high degree of similarity between **Figure 12** showing the total amount of material in the nozzle-throat region and **Figure 5** showing the outflow from the nozzle. However, in the low flow regions the curve for the accumulation of material (**Figure 12**) typically leads the curve for flow rate (**Figure 5**) by 1-5 ms.

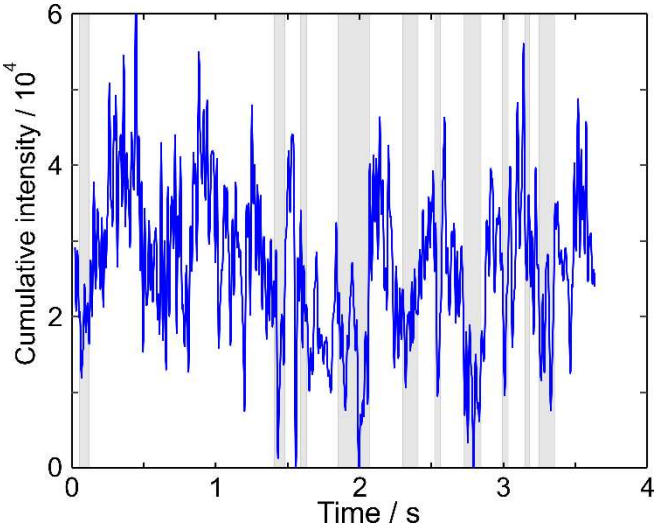

Figure 12. Cumulative intensity (sum of pixel intensities) for all pixels in the wake-region, defined as being between the melt nozzle outlet and the throat. Vertical grey bars are adopted from Figure 5.

4. Discussion

The results obtained may be summarized thus:

- The gas atomizer studied can be shown to be undergoing pulsation, that is the volume of melt instantaneously being delivered to the nozzle tip, is undergoing large amplitude, chaotic variation.
- During periods of high melt flow the velocity of material in the melt plume is of the order of 40 m s^{-1} as it is stripped off the nozzle tip, dropping to around 15 m s^{-1} at a distance of 9.5 mm downstream from the nozzle. Thereafter the velocity is approximately constant until the plume ceases to be visible.
- During these periods of high melt flow the melt plume has a well-developed constriction, or throat, which is on average 3.79 mm in diameter and 3.17 mm downstream of the nozzle tip.
- During periods of low melt flow the velocity of material as it is stripped of the nozzle tip is of the order of 15 m s^{-1}, a velocity which remains more-or-less constant as the material moves downstream.
- During the period of low melt flow the throat in the melt plume is narrower and its average is further downstream, with the mean throat diameter being 3.25 mm and its average location being 3.80 mm below the nozzle tip.

The results with respect to the relationship between melt velocity, throat diameter and throat position, all as a function of optical brightness, which is here taken as a proxy for the volume flow rate of the metal, are summarized in **Figure 13**. Each of the three curves in **Figure 13** has been obtained by performing non-linear regression over all 65536 measurements and plotting the resulting trends lines to represent the average dependence upon optical brightness. Our contention is that all of these observations are consistent with the physical mechanism giving

rise to pulsation being an oscillation between the open- and closed-wake conditions. Specifically, the closed-wake is terminated by a Mach disk, a shock structure at which the gas velocity is reduced. Consequently, melt passing through the closed-wake may well be travelling more slowly than that passing through the open-wake, as in the closed-wake condition the melt must exit the recirculation zone through the Mach disk, wherein it is decelerated. Moreover, it is clear that, with reference to **Figure 1**, the presence of the Mach disk in the closed-wake condition causes the constriction at the termination of the recirculation zone to narrow and move further downstream.

While **Figure 1** is strictly valid in the case of gas only flow, the data presented here appears to indicate that some clear vestige of these structures are able to survive the passage of the melt through the recirculation zone. As such, we contend that it is perfectly valid to discuss the presence of both the open- and closed-wake during two-phase flow in a close-coupled gas atomizer. The features associated with the closed-wake seem to correlate well with periods of low melt flow in the atomizer and that conversely the features associated with the open-wake seem to correlate well with periods of high melt flow. Moreover, the total quantity of melt contained within the wake-region, defined here as the region between the nozzle and the throat, also correlates well with the melt flow-rate from the nozzle. However, the melt flow-rate lags the total quantity of melt by between 1-5 ms. We suggest that if the lowering of the melt flow-rate is due to the high back-pressure exerted by the closed-wake condition, the lag may be explained by an accumulation of melt in the wake region causing the disruption of the closed-wake, as first proposed by Ting et al. (2002). Once the closed-wake were disrupted the back-pressure would drop and the melt flow-rate would increase, giving a natural explanation for the observed lag.

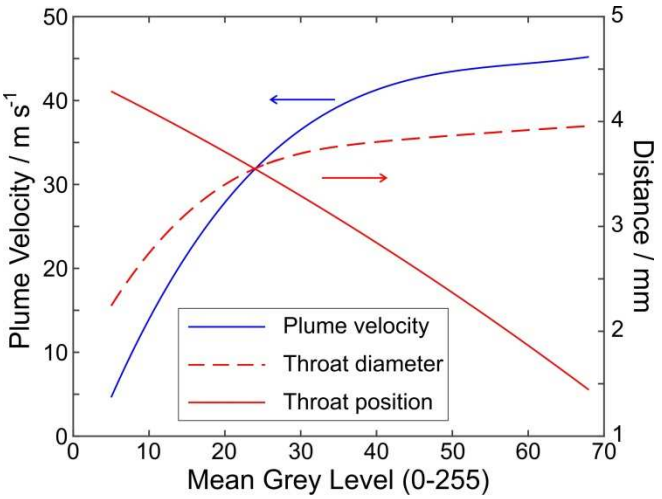

Figure 13. Best estimate, based upon regression analysis, of the plume velocity, throat diameter and throat position as a function of mean grey level through a window located 5 pixels below the nozzle outlet, taken here as a proxy (arbitrary units) for the melt flow rate.

Consequently we contend that, unlike the assertion of Mates and Settles (2005a, 2005b), the closed-wake condition can exist during the atomization of a second fluid in the close-coupled atomization configuration and that alternation between the open- and closed-wake configuration is intimately related to the melt pulsation phenomenon observed during atomization. This suggests possible lines of enquiry in the development of gas atomization equipment. Specifically, if the wake condition could be stabilized, pulsation could be reduced which should in turn lead to a narrower powder size distribution. This paper presents a methodology by which the stability of the wake condition can be measured during two-phase flow, and hence by which design modification can be assessed. Even within existing atomization technology, small changes in the atomizer configuration can alter the wake closure pressure by almost a factor of 2 (Motaman et al., 2015) and, as far as we are aware, the relative stability of the closed-wake as a function of wake closure pressure, and hence the PSD, have not been investigated.

Acknowledgements

This work was funded by MAPP – The EPSRC Future Manufacturing Hub in Manufacture using Advanced Powder Process (Grant No. EP/P006566/1).

5. References

Anand, V., Kaufman, A.J. and Grant, N.J., Rapid Solidification of a Modified 7075 Aluminum Alloy by Ultrasonic Atomization, in *Rapid Solidification Processing, Principles & Technologies II*, Mehrabian, R., Kear, B.H., Cohen, M. Eds., Claitor, Baton Rouge, pp. 273-286, 1980.

Anderson, I.E., Figliola, R.S. and Morton, H., Flow Mechanisms in High Pressure Gas Atomization, *Mater. Sci. Eng. A*, vol. **148**, no. 1, pp. 104-114, 1991.

Anderson, I.E. and Terpstra, R.L., Progress towards gas atomisation processing with increased uniformity and control, *Mater. Sci. Eng. A*, vol. **326**, no. 1, pp. 101-109, 2002.

Anderson, I.E., Terpstra, R.L., Cronin, J.A., Figliola, R.S., Verification of melt property and closed wake effects on controlled close-coupled gas atomisation processes, in *Advances in Powder Metallurgy and Particulate Materials*, Gasbarre, W.R., von Arx, J.W. Eds., Metal Powder Industries Fed., pp. 1-16, 2006.

Anderson, I.E., White, E.M.H. and Dehoff, R., Feedstock powder processing research needs for additive manufacturing development, *Curr. Opin. Solid State Mater. Sci.*, vol. **22**, no. 1, pp. 8-15, 2018.

Duke, D., Honnery, D. and Soria, J., A cross-correlation velocimetry technique for breakup of an annular liquid sheet, *Exp. Fluids*, vol. **49**, no. 2 pp. 435-445, 2010.

Ejiri, Y., Hamada, N., Moving object velocity estimation using feature point image, *TENCON 2006 - IEEE Region 10 Conference, Hong Kong*, IEEE: New York, 2006.

Lubanska, J., Correlation of spray ring data for gas atomisation of liquid metals, *J. Metals*, vol. **22**, no. 2, pp. 45-49, 1970.

Malavika, T. and Poornima, M., Moving object detection and velocity estimation using MATLAB, *Int. J. Eng. Res. Technol.*, vol. **2**, no. 1, pp. 1-4, 2013.

Mates, S.P. and Settles, G.S., A flow visualisation study of the gas dynamics of liquid atomisation nozzles, in *Advances in Powder Metallurgy and Particulate Materials*, Metal Powder Industries Fed., vol. **1**, pp. 15-29, 1995.

Mates, S.P. and Settles, G.S., A study of liquid metal atomization using close-coupled nozzles, Part2: Atomization behaviour, *Atomization Sprays*, vol. **15**, no. 1, pp. 41-59, 2005a.

Mates, S.P. and Settles, G.S., A study of liquid metal atomization using close-coupled nozzles, Part 1: Gas dynamic behaviour, *Atomization Sprays*, vol. **15**, no. 1, pp. 19-40, 2005b.

Motaman, S., Mullis, A.M., Cochrane, R.F. and Borman, D.J., Numerical and experimental investigation of the effect of melt delivery nozzle design on the open- to closed-wake transition in closed-coupled gas atomization, *Metall. Mater. Trans. B*, vol. **46**, no. 4, pp. 1990-2004, 2015.

Mullis, A.M., Adkins, N.J., Aslam, Z., McCarthy, I.N. and Cochrane, R.F., Close-Coupled Gas Atomization: High Frame Rate Analysis Of Spray Cone Geometry, *Int. J. Powder Metall.*, vol. **44**, no. 1, pp. 55-64, 2008.

Mullis, A.M., McCarthy, I.N. and Cochrane, R.F., High speed imaging of the flow during close-coupled gas atomisation: Effect of melt delivery nozzle geometry, *J. Mater. Process Technol.*, vol. **211**, no. 9, pp. 1471-1477, 2011.

Mullis, A.M., McCarthy, I.N., Cochrane, R.F. and Adkins, N.J., Log-normal melt pulsation in close-coupled gas atomization, *Metall. Mater. Trans. B*, vol. **44**, no. 4, pp. 789-793, 2013.

Ting, J. and Anderson, I.E., Computational fluid dynamics (CFD) investigation of wake closure phenomena, *Mater. Sci. Eng. A*, vol. **379**, no. 1-2, pp. 264-276, 2004.

Ting, J., Connor, J. and Ridder, S., High-speed cinematography of gas-metal atomization, *Mater. Sci. Eng. A*, vol. **390**, no. 1-2, pp. 452–460, 2005.

Ting, J., Peretti, M.W. and Eisen, W.B., The effect of wake-closure phenomenon on gas atomization performance, *Mater. Sci. Eng. A*, vol. **326**, no. 1, pp. 110-121, 2002.

Tokumura, P.T. and Dimotakis, P.E., Image correlation velocimetry, *Exp. Fluids*, vol. **19**, no. 1, pp. 1-15, 1995.

Zhao, X., Xu, J., Zhu, X., Zhang, S., Effect of atomisation gas pressure variation on the gas flow field in the supersonic gas atomisation, *Sci. China, Ser. E*, vol. **52**, no. 10 pp. 3046-3053, 2009.